Check for updates

Moisture changes inside hydrogel particles during their drying process investigated with fluorescence lifetime imaging†

Sankar Jana 🆔 and Dominik Wöll 🆔 *

The properties of hydrogels and microgels, *i.e.* hydrogel particles, depend strongly on their water content. Based on our previously developed method to access the local water content in microgels, we performed fluorescence lifetime microscopy measurements at different stages of drying poly(*N*-isopropylacrylamide) (PNIPAM) microgels under ambient conditions. For this purpose, the red-emitting dye ATTO 655 was covalently attached to the microgels. Its emission is quenched by water molecules due to an energy transfer from the first excited state of the dye to a vibrational level of the water molecules. The quenching constant or, equivalently, the fluorescence lifetime, gives direct access to the local water concentration. We measured the fluorescence lifetime after spin-coating, reswelling and at different times of subsequent drying to follow the changes of water content during this process. We found that the microgels are not totally dry after spin coating, but drying them to their equilibrium moisture under ambient temperature and humidity conditions requires several hours. Additionally, we determined the moisture inside microgels in equilibrium at different air humidities. In summary, the method allows for a detailed investigation of the moisture inside hydrogels and gives straight-forward access to *in situ* and operando measurements of hydrogel systems.

1 Introduction

Hydrogels represent a fascinating class of materials with a plethora of applications, including in the fields of medicine,[1] agriculture,[2] and sensing.[3] A significant number of these applications necessitate the precise regulation of the swelling abilities and moisture conditions, *i.e.* the quantity of water, within the gels. When exposed to air, hydrogels inherently start to dry and the kinetics of this drying process depends on many external (*e.g.* air humidity, and temperature) and internal (*e.g.* hydrogel material and cross-linking density) parameters. Particularly, drying processes play a crucial role for small hydrogels and hydrogel particles, due to their high surface–volume ratio and the corresponding fast drying kinetics. Apart from drying the particles themselves, drying processes of small droplets containing particles[4] are essential, *e.g.*, for spray coating, spray drying ink jet printing, and nutrient and pesticide delivery.

Hydrogel particles, typically called microgels, are three-dimensional cross-linked polymer networks swollen in water.[5–7] They exhibit high potential for drug delivery including up-take, transport, and release of drugs,[8,9] (bio-)imaging,[10] tissue

engineering,[11,12] clinical applications,[13] (bio-)catalysis,[14] and sensing applications,[15,16] and as photonic materials.[17] Depending on the polymer composition, microgels can be responsive to external triggers[18] such as temperature, pH, or light. The commonly used poly(*N*-isopropylacrylamide) (PNIPAM) microgels are, for example, thermoresponsive with a volume phase transition temperature (VPTT) of 32 °C. Around this temperature, their swollen (hydrated) state changes gradually to a collapsed (dehydrated) state. However, also the addition of some co-solvents[19] and drying results in a collapse of microgels.[20] In addition, if microgels are dried on surfaces, they deform depending on their cross-linking density[21] and also on the way of deposition.[22] Since in equilibrium, a clear correlation exists between moisture in the microgel, *i.e.* the amount of water present in the microgel with respect to its total mass, and humidity of the air, microgels and hydrogels can be used for humidity sensing in the common humidity ranges,[23–25] whereas other materials and concepts are used for low humidity detection.[26] In general, humidity sensing materials have been developed based on humidity-change caused variations in electrical response,[27] hydrophobicity,[28] and resistance.[29] Also, an approach measuring the fluorescence lifetime of a ruthenium complex in the frequency domain has been reported.[30] Apart from sensing humidity, nevertheless, a further understanding of the drying process and the conditions within the microgels during this process would be facilitated by

Institute of Physical Chemistry, RWTH Aachen University, Landoltweg 2, 52074 Aachen, Germany. E-mail: woell@pc.rwth-aachen.de; Tel: +49 241 80 98624

23250 | *Phys. Chem. Chem. Phys.*, 2024, **26**, 23250–23255

This journal is © the Owner Societies 2024

knowledge of how dry microgels are under different drying conditions and drying times, and how this depends on the humidity in the air.

In previous work, it was shown that water (H_2O) molecules act as (weak) fluorescence quenchers for red-emitting dyes.[31,32] The quenching mechanism is supposed to be an energy transfer of the electronically excited state of the dye to an overtone of the O–H-stretching vibration of water molecules. As a result, the fluorescence lifetime of red-emitting dyes decreases with increasing number of water molecules around them. Recently, we applied this approach to estimate local water content within microgels with super-resolution.[33]

Here, we report on confocal fluorescence lifetime imaging (FLIM) measurements to determine the moisture/water content inside PNIPAM microgels during drying in air under typical lab environment conditions (22 °C and relative humidity of 34%). The fluorescence lifetime of ATTO 655 covalently attached to the functional amine groups of poly N-isopropylacrylamide-co-N-(3-aminopropyl)methacrylamide hydrochloride (P(NIPAM-co-APMH)) microgels (for chemical structures see Fig. S5 in the ESI†) reports on the local water concentration inside the polymer network[33] directly after spin coating, addition of a small droplet of water ($\approx$10 μL) to reswell them, and the subsequent drying process, respectively. The fluorescence lifetime values were also referenced to different relative humidity (RH) and the corresponding water content of microgels in equilibrium with the respective environment.

2 Instruments and methods

2.1 Synthesis and labeling of P(NIPAM-co-APMH) microgels

Synthesis and labeling of P(NIPAM-co-APMH) microgels can be found in our previous publications.[33] In brief, N-isopropylacrylamide (NIPAM, 97%, Acros Organics), N,N′-methylenediacrylamide (BIS, 98%, AppliChem), N-(3-aminopropyl)methacrylamide hydrochloride (APMH, 98%, Sigma), cetyltrimethylammoniumbromide (CTAB, AppliChem) and the initiator 2,2′-azobis(2-amidinopropane)dihydrochloride (V50, 97%, Sigma) and fluorescent dye ATTO 655 NHS-ester (ATTO-TEC GmbH) were used as received without further purification. Free radical polymerization was performed in a 250 mL three-necked round-bottom flask, equipped with a reflux condenser, an overhead stirrer, a thermometer, and a nitrogen inlet. The initial total monomer concentration was kept constant at 250 mM. 4.544 g of NIPAM (40.2 mmol, 93 mol%), 122.8 of mg APMH (0.86 mmol, 2 mol%) and 332.9 mg of BIS (2.16 mmol, 5 mol%) were dissolved in 168 mL of water. The oil bath was then heated up to 70 °C. The sealed apparatus was thoroughly flushed with nitrogen at least 1 h before initiation. Before free radical polymerization was initiated, the nitrogen inlet was drawn out of the liquid phase to avoid foaming and 2.4 mg of cetyltrimethylammoniumbromide (CTAB) (0.05 × the critical micellization concentration) dissolved in 2 mL degassed water was added. After initiation with 46.7 mg of V50 (1 mM in the batch) dissolved in 2.7 mL of degassed water, the initially transparent solution became progressively turbid. The mixture was allowed to react for 5 h in the

presence of nitrogen under stirring at a speed of 500 min^{-1}. To eliminate possible chemical residues, especially to remove the surfactant, the microgel dispersion was purified by ultracentrifugation (Beckman Coulter, Optima™ XPN) three times (30.000 min^{-1}, respective 21.000 × G for 1 h, where G is the gravitational constant). The supernatant was removed for each cycle, and the microgels were redispersed in double distilled water. For the covalent fluorescence labeling of P(NIPAM-co-APMH) microgels, 30 mg of the dried microgel powder was redispersed in 15 mL of water. The pH of the redispersed microgel solution was adjusted to a slightly basic value (pH 8) using 0.1 M NaOH solution to avoid undesired hydrolysis reactions. 10 μL of 4 mM ATTO 655-NHS ester in DMSO (in stoichiometric excess) was added at room temperature and allowed to react for 24 h. Unbound dye was removed again by ultracentrifugation as described earlier.

2.2 Microgel sample preparation

The ATTO 655-labeled microgel sample was resuspended in pure water. The dilute microgel samples were spin coated (4000 rpm for 40 seconds followed by 2000 rpm for 1.5 seconds at room temperature) onto a Hellmanex III-washed, plasma-cleaned coverslip. After spin coating, the coverslip was placed into the sample holder of the inverted microscope stage and FLIM images were measured. Subsequently, a drop of water ($\approx$10 μL) was placed onto the coverslip to reswell the microgel, and FLIM images were recorded at different times during the disappearance of the water drop and during the subsequent drying phase of the microgels at room temperature and a relative air humidity of 34%. Finally, the measured dry microgel sample was kept overnight at room temperature before a final FLIM measurement was performed. Additionally, we investigated the dependency of relative air humidity (RH) on the fluorescence lifetimes. For 34%, 44%, and 55% RH, the spin-coated microgel sample was equilibrated overnight in an atmosphere of the corresponding relative humidity at 22 °C. The RH values of 70 and 85% were achieved using a custom-made moisture controller with an uncertainty of ±2%. The 100% RH value was recorded for the microgel covered with water.

2.3 FLIM measurements

FLIM measurements were performed using a PicoQuant Micro-Time 200 confocal setup (PicoQuant, GmbH, Berlin, Germany) equipped with an inverted microscope (IX83, Olympus), a time-correlated single photon counting (TCSPC) unit (HydraHarp 400), and a single photon avalanche diode detector (SPAD, SPCM-AQRH, Excelitas). A pulsed NKT continuum laser (SuperK EVO, NKT Photonics) with a repetition rate of 20 MHz was used as the excitation source as outlined in our previous work.[33] For all excitations of the samples, a spectral window between 630 nm and 640 nm centered at 635 nm was chosen using a SuperK VARIA tunable filter. The laser power entering the microscope was 15 μW. A dichroic mirror (ZT633RDC-UF3, Chroma) with high reflectivity at 640 nm was used to direct the excitation light into the microscope. A 60× water immersion objective lens with NA 1.2

This journal is © the Owner Societies 2024

Phys. Chem. Chem. Phys., 2024, **26**, 23250–23255 | **23251**

(UPLSAPO60XW, Olympus, Japan) was used to focus on the sample. The sample position was adjusted using a manual XY stage (JPK Motor Stage, Olympus) and a z-piezo stage (Nano-ZL100, Mad City Labs). Fluorescence from the sample was collected with the same objective and went through the dichroic mirror. The excitation laser light was blocked in the emission path by a long-pass filter (ET655LP, Chroma). The beam was then focused onto the pinhole (100 μM P100S, Thorlabs) using an achromatic tube lens (TTL180-A, Thorlabs). It was collimated by a 100 mM focal length lens. A bandpass filter (685/75 BrightLine HC) was used directly in front of the lens. Finally, the emission light was focused onto a single photon avalanche diode (SPAD, SPCM-AQRH, Excelitas) detector. Each photon contains information regarding its arrival time and its own detection channel. The output signal of the detector was recorded using a TCSPC system (HydraHarp 400, PicoQuant) synchronized with the trigger signal of the excitation laser. The measurements were carried out using SymPho-Time 64 software (PicoQuant, GmbH, Berlin, Germany) that controlled both the TCSPC and the scanner systems. The data were stored in a time-tagged time-resolved (TTTR) mode, allowing every detected photon with its individual arrival timing and detection channel information to be recorded. All samples were measured at 22 °C. To achieve the single photon detection, we used the detection count rate at the detector of approximately 0.01% with respect to the laser excitation rate. Typically, a 10×10 μm^2 region of the sample was scanned with a pixel size of 100 nm, a dwell time of 2.5 μs per pixel, and a frame rate of 20 Hz. 3000 frames were acquired. The recorded FLIM images (typically 3000) were binned together into a single FLIM image. The overall TCSPC decay profile was extracted from the binned FLIM image after subtracting the background photon counts as described in our previous publication.[34] It was fitted with a biexponential tail fit using SymphoTime 64 software (PicoQuant, GmbH, Berlin, Germany). The fitted residuals were calculated and plotted to check the fitting quality (see the ESI†). The χ^2 values did not improve significantly when the number of decay components was increased to three.

3 Results and discussion

We investigated P(NIPAM-*co*-APMH) microgels covalently labelled with the NHS ester of ATTO 655. As shown in Fig. 1, FLIM images of these microgels deposited onto glass coverslips were recorded at the following stages. First, the FLIM image directly after spin coating was recorded (Fig. 1a). Afterwards, a small water droplet of approx. 10 μL was added which resulted in swelling of the microgels. The difference in shape between the dry and the swollen microgels can be measured by atomic force microscopy (AFM) as presented in Section S5 of the ESI.† After readjusting the focus, a FLIM image could be recorded 2 min after this addition of water. Fig. 1b illustrates a notable decline in fluorescence intensity, accompanied by a concurrent reduction in the average fluorescence lifetime (here referred to as "fast lifetime" in agreement with the definition of the
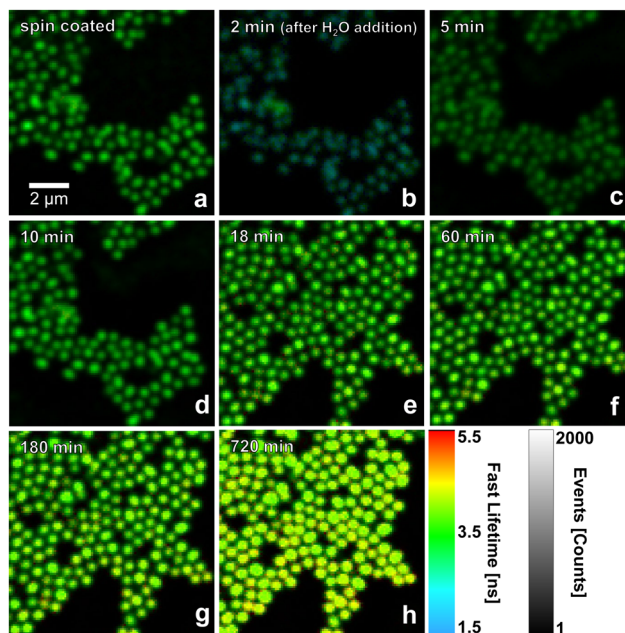

Fig. 1 Confocal FLIM images of ATTO 655 labelled P(NIPAM-*co*-APMH) microgels measured (a) after spin-coating, and (b)–(h) at different drying times (indicated in the images) at open atmospheric pressure after the addition of a small amount of H$_2$O at time zero, respectively. FLIM images of additional times are presented in Fig. S1 in the ESI.† The field of view changes between (d) and (e) since two different measurements (one concentrating on a high sampling of the short times and the other addressing the long time behaviour) were combined.

Picoquant system used to analyse the data). During the subsequent drying process under ambient conditions (22 °C and 34% RH), the fluorescence lifetime and fluorescence intensity gradually increase (Fig. 1c–h). FLIM images for additional time steps can be found in Fig. S1 of the ESI.†

TCSPC decay curves were extracted from the FLIM images. Normalized fluorescence intensity decays are presented in Fig. 2. The dotted curve shows the situation directly after spin coating. Addition of a drop of water and, thus, swelling of the microgels increases the decay rate significantly (dark blue curve). During the drying process, the fluorescence lifetimes become gradually longer. It is obvious and interesting, that the TCSPC curve directly after spin coating resembles a curve which is situated between the curves of 8 and 10 min. This, however, is not yet the end of the drying process which continued still overnight to reach the final equilibrium (red curve). This means that spin-coated microgels are not totally dry, but still contain more water than at equilibrium. The TCSPC curves were fitted with a bi-exponential decay. The resulting two fluorescence lifetimes τ_1 (red triangles) and τ_2 (blue triangles) are plotted in Fig. 3, where also the amplitude-weighted average fluorescence lifetimes $\langle\tau\rangle$ (magenta squares) and the lifetime values τ_∞ of the corresponding parameters after drying overnight are presented. All fit values including their χ^2 values are shown in Table S1 of the ESI.† During the drying process, the long component τ_1 changes from 2.89 to 4.57 ns with relative amplitudes between 56% and 66%. The short component τ_2

23252 | *Phys. Chem. Chem. Phys.*, 2024, **26**, 23250–23255
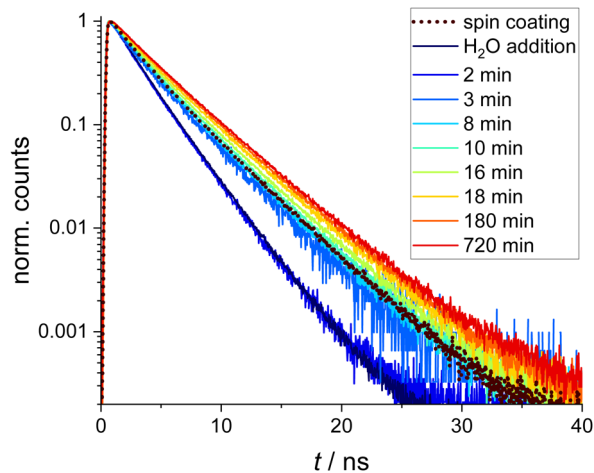
This journal is © the Owner Societies 2024

Fig. 2 Normalized TCSPC decay curves obtained from the FLIM images measured directly after spin coating (dotted black line), after addition of H_2O (dark blue line) and after different drying times, respectively. For bi-exponential fits and residuals see the ESI.†
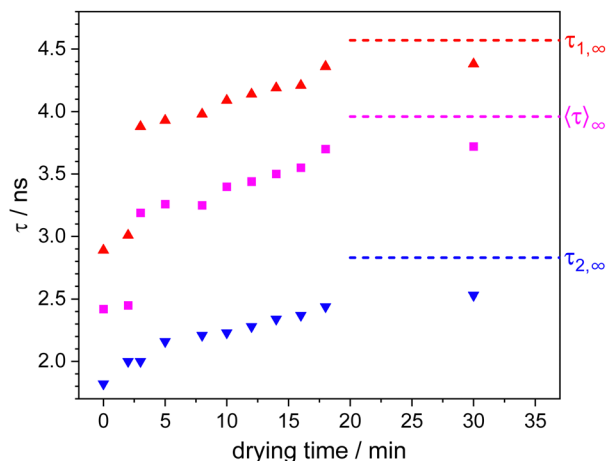

Fig. 3 Fluorescence lifetimes τ_1 and τ_2 fitted with a bi-exponential fit and amplitude-weighted average fluorescence lifetimes $\langle\tau\rangle$ for different drying times after addition of a ≈ 10 μL drop of water to spin-coated microgels. The dashed lines represent the fluorescence lifetime values obtained by a fit of the TCSPC curve measured after 720 min (overnight) drying time.

increases from 1.82 to 2.83 ns (relative amplitudes between 34% and 44%). The lifetime values of the spin-coated sample ($\tau_1 = 4.00$ ns and $\tau_2 = 2.10$ ns) resemble the ones of the sample after 8 min drying time. Both lifetime values are significantly shorter than the corresponding value of 4.57 ns and 2.83 ns in the dry state (∞), respectively. Between 2 and 3 minutes of drying time, a clear jump in the long component τ_1 can be seen, which coincides with the time when the water drop added to the coverslip evaporated completely. The short component τ_2 remains basically unaffected by this disappearance of the water drop.

The fluorescence lifetimes can be directly related to the local water content around the ATTO 655 dyes.[33] Surprisingly, the TCSPC fits required a biexponential model to be suitably fitted.

The longer and more dominant component τ_1 reaches at the end of the drying process a fluorescence lifetime value of 4.57 ns which is the fluorescence lifetime of ATTO 655 when no water or other quencher is present. The shorter lifetime component τ_2, however, points to a fraction of dyes which are either in an environment causing clearly decreased fluorescence lifetime or which have a significant amount of quencher around them. Both cases show that the surroundings in microgels, at least the ones produced by precipitation polymerization, are quite heterogeneous. A polymer density gradient from the center to the periphery is typically observed in scattering experiments.[35] Additionally, super-resolution fluorescence microscopy revealed gradients in polymer and cross-linking density[36,37] and clusters of high cross-linking density;[38] a possible explanation for which is the particle formation mechanism.[39] Also, this is in agreement with previous observations where we found some rather apolar regions inside microgels even in their swollen state.[40] Together with these previous findings, we assume that the two fluorescence lifetimes observed here originate from ATTO 655 dyes in different surroundings within the microgels. τ_1 originates from positions of the label in rather dense polymer surrounding which after applying the drop of water on top of the microgels (at times shorter than 3 min) is significantly swollen with water, which after the drop has evaporated exhibits a sudden jump and thus a rapid initial drying process between minute 2 and 3 followed by a slow further drying process over hours. The rapid initial drying process necessitates the facile diffusion of water molecules out of the microgels *via* existing percolation pathways. The loss of water results in a collapse of the polymer chains and a concomitant reduction in the polymer mesh size, thereby significantly slows down the drying process. τ_2 does not exhibit a sudden jump between 2 and 3 minutes of drying time. This may indicate that the higher amount of water in these surroundings cannot leave quickly enough and becomes entrapped by the collapsing polymer chains in consistency with the time evolution of τ_1.

The quick speed of the drying process and the missing possibility to use switching buffers prevent us from applying localization-based super-resolution methods to access local single molecule properties. However, we are planning ways to gain deeper insights, but these are beyond the scope of this paper.

Finally, with the novel tool of moisture sensing at our disposal, we conducted a series of experiments at different relative air humidities after allowing sufficient time for equilibration. The corresponding TCSPC decay curves were again fitted with a bi-exponential model (see Section S3 of the ESI†). The resulting fluorescence lifetime values are plotted in Fig. 4 and presented in Table S2 (ESI†). All fluorescence lifetime values can be reasonably well-fitted with linear functions. Applying this calibration to the spin coated microgels suggests that the moisture inside spin coated microgels is similar to the moisture inside microgels in equilibrium with 70% relative air humidity. In addition, we can connect for each drying time, the fluorescence lifetime values of Fig. 3 to corresponding water
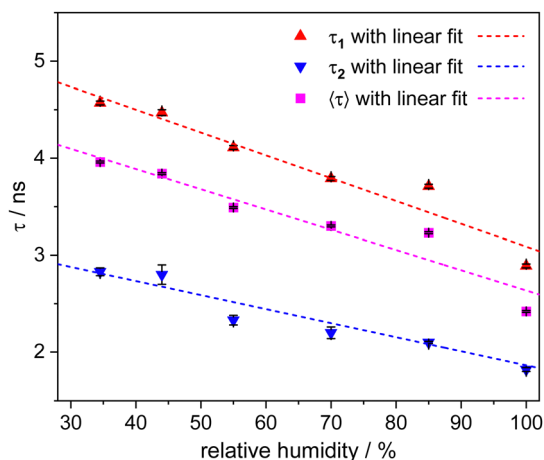
This journal is © the Owner Societies 2024

Phys. Chem. Chem. Phys., 2024, **26**, 23250–23255 | **23253**

Fig. 4 Plot of relative humidity *versus* the fluorescence lifetime of ATTO 655 dye labelled P(NIPAM-*co*-APMH) microgels. τ_1 and τ_2 are the lifetimes obtained by a bi-exponential fit of the fluorescence decay curves. The fit values can be found in Table S2 of the ESI.† $\langle\tau\rangle$ is the average fluorescence lifetime calculated from the amplitude-weighted average of τ_1 and τ_2. The data points for τ_1, τ_2, and $\langle\tau\rangle$ have been fitted using three linear equations: $\tau_1 = 5.44 - 0.023 \times RH$, $\tau_2 = 3.31 - 0.014 \times RH$, and $\langle\tau\rangle = 4.72 - 0.021 \times RH$, respectively.

contents as they would be found when equilibrated at specific relative air humidities. Although RH can be determined with greater ease and at a lower cost for macroscopic systems, our method of measuring humidity at the local level in the very small volume defined by the microgels offers significant advantages for micro- and nanoscopic systems.

4 Conclusions

We presented a novel method for determining the moisture inside hydrogels and here, in particular, microgels. It utilizes the fact that the fluorescence lifetime of red-emitting fluorophores is sensitive to water molecules in their vicinity, and it allowed us to follow the drying process of ATTO 655-labelled PNIPAM microgels from the swollen state in water to the dry state after reaching equilibrium after several hours in a room with well-defined air humidity. After the water outside the microgels has evaporated, the moisture inside the gels drops rapidly. However, after this initial drop, it takes several hours to reach equilibrium with ambient humidity. In addition, we determined how the fluorescence lifetime in microgels at equilibrium depends on the air humidity and found a linear dependency. Thus, we can connect the moisture inside microgels at different times of the drying state to the equilibrium moisture at corresponding relative air humidity. Also, we were able to show that the moisture in the microgels studied here immediately after spin-coating was equivalent to equilibrium moisture at 70% relative humidity. Apart from finding out about the moisture in the microgels, the method could be used to sense humidity for example in the small volumes of nanodevices.

Author contributions

D. W. carried out the conceptualization. S. J. and D. W. designed the experiments. S. J. performed all the experiments and S. J. and D. W. analyzed data. D. W. and S. J. wrote the manuscript. All authors read and approved the final manuscript.

Data availability

Data are stored according to the guidelines of the DFG. Additional data are available upon request.

Conflicts of interest

There are no conflicts to declare.

Acknowledgements

Notes and references

1 S. Correa, A. K. Grosskopf, H. Lopez Hernandez, D. Chan, A. C. Yu, L. M. Stapleton and E. A. Appel, *Chem. Rev.*, 2021, **121**, 11385–11457.

2 I. Piccoli, C. Camarotto, A. Squartini, M. Longo, S. Gross, M. Maggini, M. L. Cabrera and F. Morari, *Agron. Sustainable Dev.*, 2024, **44**, 22.

3 X. Sun, S. Agate, K. S. Salem, L. Lucia and L. Pal, *ACS Appl. Bio. Mater.*, 2021, **4**, 140–162.

4 R. G. Larson, *AIChE J.*, 2014, **60**, 1538–1571.

5 F. A. Plamper and W. Richtering, *Acc. Chem. Res.*, 2017, **50**, 131–140.

6 M. Karg, A. Pich, T. Hellweg, T. Hoare, L. A. Lyon, J. J. Crassous, D. Suzuki, R. A. Gumerov, S. Schneider, I. Potemkin and W. Richtering, *Langmuir*, 2019, **35**, 6231–6255.

7 F. Scheffold, *Nat. Commun.*, 2020, **11**, 4315.

8 X. Peng, Q. Peng, M. Wu, W. Wang, Y. Gao, X. Liu, Y. Sun, D. Yang, Q. Peng, T. Wang, X.-Z. Chen, J. Liu, H. Zhang and H. Zeng, *ACS Appl. Mater. Interfaces*, 2023, **15**, 19560–19573.

9 T. R. Hoare and D. S. Kohane, *Polymer*, 2008, **49**, 1993–2007.

10 Q. M. Zhang, W. Wang, Y.-Q. Su, E. J. M. Hensen and M. J. Serpe, *Chem. Mater.*, 2016, **28**, 259–265.

11 G. Agrawal and R. Agrawal, *Small*, 2018, **14**, 1801724.

12 Q. Feng, D. Li, Q. Li, X. Cao and H. Dong, *Bioact. Mater.*, 2022, **9**, 105–119.

23254 | *Phys. Chem. Chem. Phys.*, 2024, **26**, 23250–23255

This journal is © the Owner Societies 2024

13 Y. Kittel, A. J. C. Kühne and L. De Laporte, *Adv. Healthcare Mater.*, 2022, **11**, e2101989.

14 S. Wiese, A. C. Spiess and W. Richtering, *Angew. Chem., Int. Ed.*, 2013, **52**, 576–579.

15 S. Su, M. M. Ali, C. D. M. Filipe, Y. Li and R. Pelton, *Biomacromolecules*, 2008, **9**, 935–941.

16 M. R. Islam, A. Ahiabu, X. Li and M. J. Serpe, *Sensors*, 2014, **14**, 8984–8995.

17 D. Menne, F. Pitsch, J. E. Wong, A. Pich and M. Wessling, *Angew. Chem., Int. Ed.*, 2014, **53**, 5706–5710.

18 G. Del Monte, D. Truzzolillo, F. Camerin, A. Ninarello, E. Chauveau, L. Tavagnacco, N. Gnan, L. Rovigatti, S. Sennato and E. Zaccarelli, *Proc. Natl. Acad. Sci. U. S. A.*, 2021, **118**, e2109560118.

19 S. Bharadwaj, B. J. Niebuur, K. Nothdurft, W. Richtering, N. F. A. van der Vegt and C. M. Papadakis, *Soft Matter*, 2022, **18**, 2884–2909.

20 K. Horigome and D. Suzuki, *Langmuir*, 2012, **28**, 12962–12970.

21 A. Scotti, M. F. Schulte, C. G. Lopez, J. J. Crassous, S. Bochenek and W. Richtering, *Chem. Rev.*, 2022, **122**(13), 11675–11700.

22 L. Hoppe Alvarez, A. A. Rudov, R. A. Gumerov, P. Lenssen, U. Simon, I. I. Potemkin and D. Wöll, *Phys. Chem. Chem. Phys.*, 2021, **23**, 4927–4934.

23 M. R. Islam, S. Xie, D. Huang, K. Smyth and M. J. Serpe, *Anal. Chim. Acta*, 2015, **898**, 101–108.

24 D. Buenger, F. Topuz and J. Groll, *Prog. Polym. Sci.*, 2012, **37**, 1678–1719.

25 M. R. Islam and M. J. Serpe, *RSC Adv.*, 2014, **4**, 31937–31940.

26 Z. Ma, T. Fei and T. Zhang, *Sens. Actuators, B*, 2023, **376**, 133039.

27 H. Zhao, X. Lin, R. Qi, J. Dai, S. Liu, T. Fei and T. Zhang, *IEEE Sens. J.*, 2019, **19**, 833–837.

28 J. Dai, T. Zhang, H. Zhao and T. Fei, *Sens. Actuators, B*, 2017, **242**, 1108–1114.

29 W. Dong, Z. Ma and Q. Duan, *Sens. Actuators, B*, 2018, **272**, 14–20.

30 O. McGaughey, J. V. Ros-Lis, A. Guckian, A. K. McEvoy, C. McDonagh and B. D. MacCraith, *Anal. Chim. Acta*, 2006, **570**, 15–20.

31 J. Maillard, C. A. Rumble and A. Fürstenberg, *J. Phys. Chem. B*, 2021, **125**, 9727–9737.

32 J. Maillard, K. Klehs, C. Rumble, E. Vauthey, M. Heilemann and A. Fürstenberg, *Chem. Sci.*, 2021, **12**, 1352–1362.

33 S. Jana, O. Nevskyi, H. Höche, L. Trottenberg, E. Siemes, J. Enderlein, A. Fürstenberg and D. Wöll, *Angew. Chem., Int. Ed.*, 2024, **63**, e202318421.

34 S. Thill, T. Schmidt, S. Jana, D. Wöll and R. Gebhardt, *Macromol. Mater. Eng.*, 2022, **307**, 2200272.

35 M. Stieger, W. Richtering, J. S. Pedersen and P. Lindner, *J. Chem. Phys.*, 2004, **120**, 6197–6206.

36 S. Bergmann, O. Wrede, T. Huser and T. Hellweg, *Phys. Chem. Chem. Phys.*, 2018, **20**, 5074–5083.

37 E. Siemes, O. Nevskyi, D. Sysoiev, S. K. Turnhoff, A. Oppermann, T. Huhn, W. Richtering and D. Wöll, *Angew. Chem., Int. Ed.*, 2018, **57**, 12280–12284.

38 A. A. Karanastasis, Y. Zhang, G. S. Kenath, M. D. Lessard, J. Bewersdorf and C. K. Ullal, *Mater. Horiz.*, 2018, **5**, 1130–1136.

39 O. L. J. Virtanen, M. Kather, J. Meyer-Kirschner, A. Melle, A. Radulescu, J. Viell, A. Mitsos, A. Pich and W. Richtering, *ACS Omega*, 2019, **4**, 3690–3699.

40 A. Purohit, S. P. Centeno, S. K. Wypysek, W. Richtering and D. Wöll, *Chem. Sci.*, 2019, **10**, 10336–10342.

This journal is © the Owner Societies 2024

Phys. Chem. Chem. Phys., 2024, **26**, 23250–23255 | **23255**